Pakistan Veterinary Journal

ISSN: 0253-8318 (PRINT), 2074-7764 (ONLINE)
DOI: 10.29261/pakvetj/2024.291

RESEARCH ARTICLE

Comparative Efficacy of Pharmacological Agents in the Ablation of Subcutaneous Insulinomas in Nude Mice Models

Nan Yi[1, #], Fengping Chen[2, #], Biaolin Zheng[2], Wenwen Guo [3], Lin Yu[4], Shanyu Qin[2, *] and Haixing Jiang[2, *]

[1]Department of Gastroenterology, The First Affiliated Hospital of Guangxi Medical University, Nanning, China; Guangxi Medical University, Nanning, China; Department of Gastroenterology, The People's Hospital of Guangxi Zhuang Autonomous Region, Nanning, China.[2]Department of Gastroenterology, The First Affiliated Hospital of Guangxi Medical University, Nanning, China. Guangxi Medical University, Nanning, China.[3]Department of Pathology, The People's Hospital of Guangxi Zhuang Autonomous Region, Nanning, China.[4]Department of Animal Genetics and Breeding, Animal Science and Technology College, Guangxi University, Nanning, China.
[#] These authors contributed equally to this study.
*Corresponding author: Jianghaixing@gxmu.edu.cn; qinshanyu@gxmu.edu.cn

ARTICLE HISTORY (24-633)

Received: October 10, 2024
Revised: November 28, 2024
Accepted: December 2, 2024
Published online: December 9, 2024

Key words:
Anhydrous ethanol
Lauromacrogol
Insulinoma
Paclitaxel
Polidocanol

ABSTRACT

Endoscopic ultrasound-guided local ablation therapy is one of the most important approaches for treating insulinomas that arise from neuroendocrine islet cell tumors located within the pancreas. This study aimed to evaluate the efficacy of various ablative treatments including anhydrous ethanol, lauromacrogol, polidocanol, and paclitaxel as local ablative agents on subcutaneous insulinoma tumors in mice models using tumor necrosis and drug distribution. For this purpose, mice were modeled for insulinoma tumors by subcutaneous injection of Ins-1 and Min-6 cell lines in 4-6 weeks-old nude female mice. The tumors became visible 1 to 2 weeks after the transplantation of cells, reaching a treatment-appropriate volume of 20-30mm^3 within 2 to 3 weeks, as confirmed by the insulinoma-like characteristics observed during histopathological analysis. The results indicated that the insulinoma animal models exhibited an early onset of hypoglycemia and significantly elevated serum insulin levels during starvation tests, compared to the control group further confirmed by expression of chromogranin A (CgA), synaptophysin (Syn), and insulinoma-associated protein 1 (Insm1) in the tumor cells during immunohistochemical staining. Following treatment, necrosis percentages in insulinoma tumors were significantly higher in the paclitaxel (93.2%) and ethanol (86.5%) groups compared to saline, polidocanol, and polyglactin groups. Similarly, tumor drug distribution was tracked using methylene blue, with paclitaxel demonstrating the fastest diffusion, followed by ethanol, polidocanol, and polyglactin. These findings suggest that both paclitaxel and polidocanol have significant potential as local ablative agents in inducing tumor necrosis, with paclitaxel offering the fastest drug dispersion. These results highlight the potential for further optimization of ablation therapies in insulinoma treatment.

To Cite This Article: Yi N, Chen F, Zheng B, Guo W, Yu L, Qin S and Jiang H, 2024. Comparative Efficacy of Pharmacological Agents in the Ablation of Subcutaneous Insulinomas in Nude Mice Models. Pak Vet J. http://dx.doi.org/10.29261/pakvetj/2024.291

INTRODUCTION

Insulinomas are functional neuroendocrine tumors that arise from neuroendocrine islet cells or pluripotent stem cells within the pancreas. The estimated annual incidence rate in humans is over 3 million cases (Tsang *et al*., 2016). In contrast, the incidence rate of insulinomas in animals varies by species, with sporadic cases reported in ferrets, dogs, and cats (Hawks *et al*., 1992; Buishand, 2022). While the majority of insulinomas in humans are benign, they often present as malignant in dogs and ferrets, with a malignancy rate of 95%. These tumors are frequently associated with severe imbalances in blood glucose levels and insulin secretion (de Herder *et al*., 2006; Greene and Bright, 2008; Bełtowski *et al*., 2018; Ryan *et al*., 2021; Kornya *et al*., 2022), leading to complications such as hypoglycemic coma, seizures, ataxia, and behavioral changes (Varela *et al*., 2018; Scott

In Press

and Howe, 2019; Sato *et al*., 2024). In animals, these tumors can significantly affect health, particularly in companion animals, where cases of insulinoma have been documented across various species (Hess *et al*., 2013; Yau and Rissi, 2014; Binici *et al*., 2016; Foxx *et al*., 2022).

The management of insulinomas presents unique challenges due to limited treatment options and the tumor's endocrine nature, which complicates efforts to effectively ablate the tumor while preserving surrounding tissue (Gómez Ochoa *et al*., 2021; Hendricks-Wenger *et al*., 2022). In both veterinary and human medicine, surgical resection of the tumor remains the standard procedure; however, it is associated with a high risk of trauma and compromised pancreatic function in later stages (Miwa *et al*., 2009; Jilesen *et al*., 2016; Crinò *et al*., 2023). Alternatively, minimally invasive procedures, such as endoscopic ultrasound-guided ethanol ablation (EUS-EA) and radiofrequency ablation, have shown promising results by reducing complications and procedural costs while providing symptomatic relief in various clinical cases. (Qin *et al*., 2014; Crinò *et al*., 2023; Matsumoto and Kato, 2023). Anhydrous ethanol ablates tumor tissue through mechanisms of cellular dehydration and denaturation. Its high permeability enables ethanol to rapidly penetrate cell membranes, resulting in the loss of intracellular water and subsequent cell death. Additionally, ethanol can induce protein coagulation and vasoconstriction, thereby reducing blood supply to the tumor and enhancing therapeutic efficacy. However, the use of ethanol is limited by the potential for ulcerative complications in adjacent tissues, peritonitis, pancreatic pseudocysts, and hematomas (Mehrabi *et al*., 2014; Matsumoto and Kato, 2023).

Nevertheless, there have been no successful cases of ablative treatment using a single agent alone for neoplastic lesions in the pancreas (Moyer *et al*., 2017). Therefore, in order to enhance efficacy and safety, alternative local ablative agents, including lauromacrogol, polidocanol, and paclitaxel, are being explored. Lauromacrogol induces tissue ablation through chemical necrosis, primarily causing apoptosis or necrosis by disrupting cell membranes and intracellular structures. Polidocanol, a surfactant, exerts its ablation effect by compromising the integrity of cell membranes. It reduces the surface tension of the membrane, leading to the leakage of cellular contents and ultimately resulting in cell death. Additionally, paclitaxel is a microtubule inhibitor that suppresses cell division by disrupting the dynamic stability of microtubules. It promotes microtubule polymerization, thereby blocking the normal progression of the cell cycle and inducing apoptosis in tumor cells. Although lauromacrogol, polidocanol, and paclitaxel show promise in ablation therapies, they lack extensive clinical data regarding their efficacy, dosing, and side effects, particularly in large-scale studies (Gaballa *et al*., 2019; Gallo *et al*., 2022). Consequently, there is an urgent need to identify gaps in knowledge, optimize dosing strategies, and evaluate long-term outcomes through further investigation. The current study aims to evaluate the comparative efficacy of four pharmacological agents including anhydrous ethanol, polidocanol, lauromacrogol, and paclitaxel in ablating subcutaneous insulinomas in a nude mouse model. Additionally, this study will assess the necrosis rates, diffusion properties, and adverse effects associated with these local ablative agents, seeking insights into safer and more effective alternatives for the treatment of insulinoma in both humans and veterinary medicine.

MATERIALS AND METHODS

Ethical statement: The study was conducted after the ethical approval of the "Animal Experimentation Ethics Committee" of Guangxi Medical University (approval number: 2023-E248-01). The study adhered to *Guiding Opinions on the Treatment of Laboratory Animals* issued by the Ministry of Science and Technology as well as the *Laboratory Animal Guideline for Ethical Review of Animal Welfare* issued by the National Standard GB/T35892-2018 of the People's Republic of China.

Procurement of chemicals: Fetal bovine serum was purchased from Biological Industries (BI, Kibbutz Beit Haemek, Israel). RPMI 1640 medium was purchased from Gibco (Shanghai, China). Penicillin-streptomycin was purchased from Thermo Fisher Scientific (Waltham, MA, USA). The 0.25% trypsin digestion solution with EDTA was purchased from Solarbio Life Sciences (Beijing, China). The lauromacrogol injection reagent was obtained from Shaanxi Tianyu Pharmaceutical Co., Ltd (Shaanxi, China. The anhydrous ethanol injection reagent was obtained from National Pharmaceutical Group Guorui Pharmaceutical Co., Ltd (Anhui, China). The 1% polidocanol injection reagent (2 mL: 20 mg) was acquired from Hameln Pharmaceuticals GmbH (Hameln, Germany), and paclitaxel (10 mL: 60 mg) was obtained from Jiangsu Aosaikang Pharmaceutical Co., Ltd (Jiangsu, China).

Cell culture: The insulinoma cell lines Ins-1 and Min-6 were obtained from Procell Life Sciences & Technology Co., Ltd. (Wuhan, China). These cells were cultured in RPMI 1640 medium containing 10% fetal bovine serum and 1% penicillin-streptomycin, and grown in a humidified incubator using 5% CO_2 and 37°C. In this study, the number of cell passages was kept below 30.

Tumor models: In this study, SPF-grade female Balb/c mice (20 ± 2g, 4−6 weeks-old) were obtained from the Animal Experimental Centre of Guangxi Medical University (Nanning, China).

A total of 1×10^7 Ins-1 cells were subcutaneously injected into the dorsal region of 4-6 weeks-old BALB/c nude mice to establish a subcutaneous tumor model. Following the implantation of cells, tumor nodules became visible at the injection site and were observed by the naked eye. Tumor size was measured every 2 days, and a tumor growth curve was plotted accordingly. The body weight and tumor volume of each mouse were recorded before the surgery. For each tumor, three morphological dimensions (L: length, W: width, and H: height) were measured. The volume of each tumor was estimated using the formula for an ellipse:

$$V=\pi LWH/6$$

Once the subcutaneous tumors reached a diameter of 8-10 mm, the mice were subjected to fasting, and

starvation tests were initiated. Blood glucose levels were measured every 3-4 hours using a blood glucose meter (Accu-Chek; Roche, Basel, Switzerland). The starvation test was concluded when the blood glucose level dropped below 2.8mmol/L, at which point plasma insulin levels were regularly measured. ELISA kit (Cloud Clone, Katy, TX, USA, Catalogue number: CEA448Mu) was used to analyze insulin levels from serum samples collected from nude Balb/c mice, detecting the absorbance at 450 nm. Each sample was assayed in triplicate, and the results were expressed as mean ± standard deviation.

Experimental design: Following the establishment of the tumor model, tumor-bearing mice were randomly divided into five groups (n=4 per group): 1. saline (control), 2. anhydrous ethanol, 3. lauromacrogol, 4. polidocanol, and 5. paclitaxel groups. The mice were anesthetized, and varying doses of all ablation agents (0.1mL, 0.15mL, 0.2mL, and 0.3mL) were injected into the central region of the tumor using an 8mm, (31G) sterile insulin syringe (Shanghai Kindly Medical Instruments Co., Ltd., Shanghai, China) at a controlled infusion rate of approximately 0.1mL every 30 seconds, ensuring bloodless draw of the needle injection. Experiments that included significant drug spillage were excluded from the study. Following the procedure, mice were housed in an SPF facility and were monitored for feeding behavior and any signs of skin surface breakage, crusting, or infection at the tumor site.

Tumor necrosis rate: 72 hours post-treatment, tumors were assessed for necrosis. Briefly, mice were euthanized by intraperitoneal injection of pentobarbital (150mg/kg), and tumors were excised, weighed, and measured. The tumor tissue was sectioned into four equal pieces along the longitudinal axis and labeled as T1−T4 (Fig. 1a)**.** The tumor necrosis rate was calculated using Image-Pro Plus 6.0 (Media Cybernetics, Bethesda, MD, USA). The mean necrosis rate was determined using the weighted average method by using the following formula:

$$NR=(S-N) / S$$

where S is the total tumor area (mm^2) and N is the residual tumor area (mm^2).

Histopathological studies: For histopathological studies, sections from subcutaneous insulinomas were fixed in 10% formalin, embedded in paraffin, sectioned, and stained with Hematoxylin and Eosin for microscopic features. Each group comprised eight xenograft mice, with results validated through three independent experimental replicates.

Immunohistochemical analysis: Mounted tissue sections from the tumor were deparaffinized, rehydrated, and subjected to antigen retrieval using citrate buffer (pH 6.0) at 95°C for 30 minutes. Endogenous peroxidase activity was quenched with 3% hydrogen peroxide, and non-specific followed by blocking with 5% normal serum for 1 hour. Sections were incubated overnight at 4°C with primary antibodies against chromogranin A (CgA), synaptophysin (Syn), and insulinoma-associated protein 1 (Insm1), followed by biotinylated secondary antibodies. Detection was performed using a peroxidase-based DAB kit, and sections were counterstained with hematoxylin. The intensity of immunostaining was assessed using a light microscope and quantified with Image-Pro Plus 6.0 software (Media Cybernetics, Bethesda, MD, USA).

Drug dispersion rate: The dispersion speed of the drugs was estimated by injecting all the ablation agents: anhydrous ethanol, lauromacrogol, polidocanol, and paclitaxel after mixing with 10% methylene blue in anesthetized mice at varying doses of all ablation agents (0.1mL, 0.2mL, or 0.3mL) (n=3 per group). Thirty minutes following the methylene blue-labeled ablative drug injection, the nude mice were humanely euthanized, and tumors were bisected along the long axis, and organized by drug-dose gradient. The drug dispersion pattern was estimated through methylene blue tracing, documenting the shape, extent, and uniformity of staining. High-resolution images of tumor sections were captured using Image-Pro Plus 6.0 software for detailed analysis. The stained areas in each tumor section were quantified, and the drug dispersion rate was calculated.

Statistical analysis: SPSS statistical software (version 19.0, Chicago, IL, USA) was used for statistical analysis of the data. Data were presented as the mean ± standard deviation. Differences among multiple groups were analyzed using one-way analysis of variance (One-way ANOVA). LSD-*t*-test was used for two-way comparisons between groups while student's *t*-test was employed for comparisons between two groups. The paired t-test was used to compare the treatment outcomes before and after in the same group of animals. $P<0.05$ was considered as statistically significant.

RESULTS

The results indicated that the insulinoma animal model exhibited an earlier onset of hypoglycemia and lower blood glucose levels during the starvation test compared to the control group (without tumor) (Fig. 1 b-c). Additionally, insulin levels were significantly elevated in the insulinoma group, while the control group maintained lower mean insulin levels (Fig. 1 d). The results indicated that within 1–2 weeks post-transplantation of Ins-1 and Min-6 cells subcutaneously, tumors became visible and exhibited exponential growth, reaching a treatment-appropriate volume within 2–3 weeks (Fig. 2 a).

Histopathological studies: During histopathological examination, the transplanted tumors exhibited pathological features resembling that of insulinoma. The tumor cells were observed to be arranged in nests of clusters, with strips of interstitium rich in blood sinusoids. The nuclei exhibited fine chromatin with inconspicuous nucleoli. Besides, the nuclei had one nuclear schism/10 high power field (HPF), and no necrosis was seen (Fig. 2 b).

Immunohistochemical analysis: Immunohistochemical analyses showed that the tumor cells expressed chromophore A (CgA), synaptophysin (Syn), and insulinoma-associated protein 1 (Insm1) (Fig. 2 c).

In Press

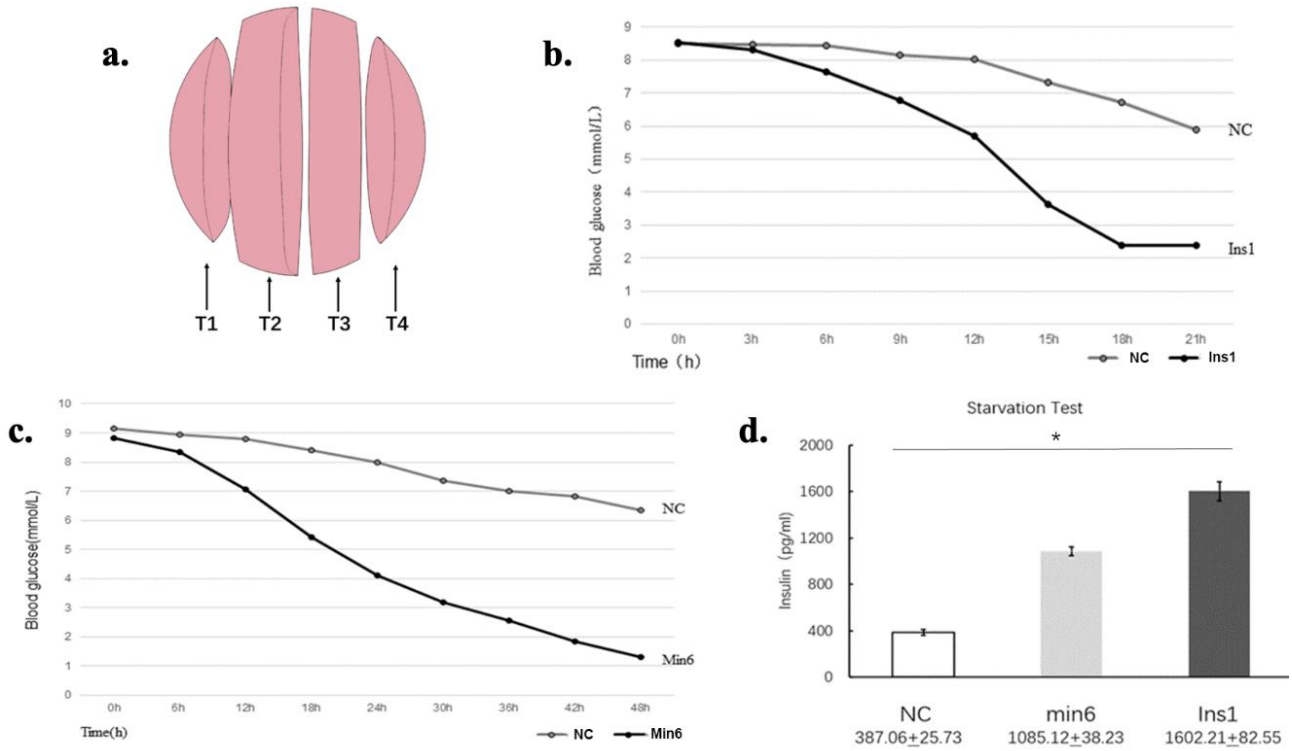

Fig. 1: Establishing animal models for insulinomas. **a.** The tumor tissue was cut into four pieces at equal distances along the long axis and labeled as T1−T4 (schematic diagram). **b.** The blood glucose levels in mice with insulinoma generated from Ins-1 cells were measured through a starvation test. **c.** The blood glucose levels in mice with insulinoma generated from Min-6 cells were measured through a starvation test. **d.** Insulin levels in the insulinoma model group after starvation test-induced hypoglycemia (pg/mL).

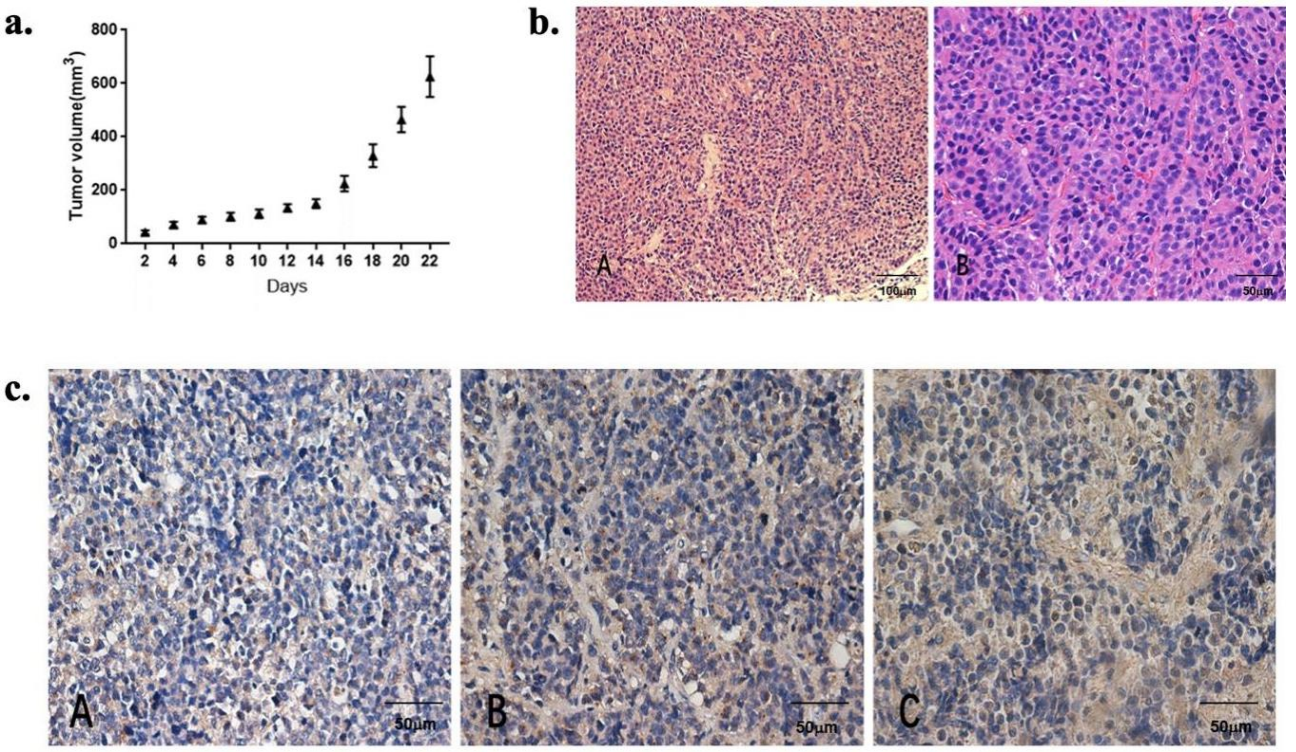

Fig. 2: Histological staining of subcutaneously transplanted tumors. **a.** The changes in the volume of subcutaneously transplanted tumors. **b.** Light micrograph after hematoxylin & eosin staining of a transplanted tumor with transplanted INS-1 cells (A: 100x; B: 200x). **c.** Immunohistochemical staining of Ins-1 generated tumors. The proteins to be detected were Cg (A), Syn (B) and Insm1 (C)

Body weight and changes in tumor-bearing nude mice: Twenty tumor-bearing nude mice that successfully underwent modeling, anesthesia, and ablation treatment, and survived 72 hours post-ablation were divided into five experimental groups. The average body weight of tumor-bearing nude mice before ablation was (19.595 ± 1.135g), with no statistically significant difference among the groups (P>0.05). In the polidocanol and normal saline

groups, the body weights of nude mice slightly increased; in the absolute ethanol group, body weight slightly decreased, while in the paclitaxel group, body weight significantly decreased (Fig. 3), showing a statistically significant difference between groups (P<0.05). Detailed changes and trends in body weight before ablation and 72 hours post-ablation are shown in Fig. 4.

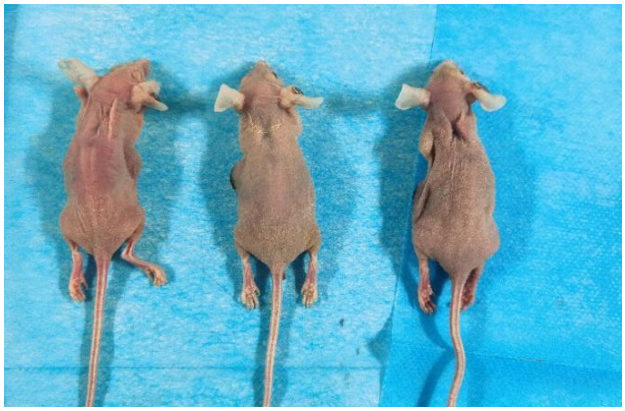

Fig. 3: Changes in body size of nude mice after ablation in the paclitaxel group. The tumor-bearing nude mice exhibited a significant decrease in body weight, a noticeable reduction in dorsal fat, skin wrinkling, and prominent visibility of the spine.

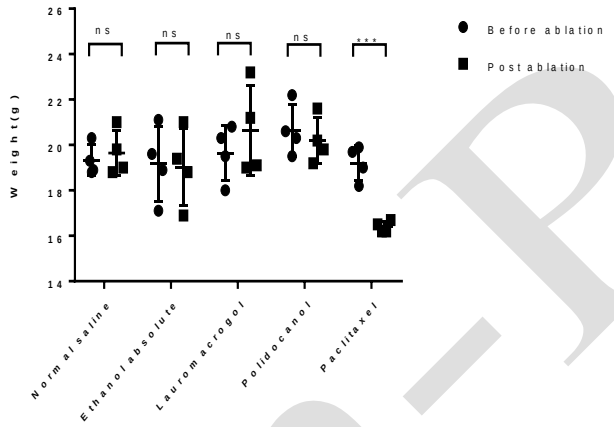

Fig. 4: Scatter plot showing the trend of weight change before and 72 hours after ablation therapy in each group. The weights are presented in (g).

Changes in tumor volume: The mean subcutaneous tumor volume in nude mice before ablation was found to be 575.31 ± 201.13 mm^3, with no statistical difference between groups (P>0.05) (Fig. 5 a). No statistical difference was found between the groups before and after ablation (P>0.05, F=2.021) (Fig. 5 b).

Necrosis Assessment: According to drug biodistribution data, the drug deposition in tumors peaked 24−48 hours after drug administration. According to the preliminary pre-test, more liquid necrosis was still visible in the section of the tumor specimen obtained 48 hours after ablation, so we finally set the observation endpoint at 72 hours after surgery, or when the tumor volume exceeded 2,000 mm^3. The focus of observation was the tumor margin zone, which generally was the junction area between necrotic tissue and the residual tumor (Fig. 5 c-f). Using a microscope, the necrotic area was characterized by irreversible nuclear lysis and nuclear division of the tumor cells, with inflammatory cell infiltration at the margins. A clear demarcation line between necrotic and tumor tissue was visible (Fig. 5 g-h).

Tumor necrosis percentages: The overall tumor area (S) and residual tumor area (N) are shown in Fig. 6 a-d. At 72 hours after ablation, the tumor necrosis percentages in each group were: paclitaxel group: 93.20 ± 8.71%, ethanol group: 86.51 ± 11.92%, polidocanol group: 70.48 ± 26.12%, polyglactin group: 34.26 ± 10.72%, and saline group: 3.29 ± 0.54%). There were significant differences in tumor necrosis rates among the five groups when 0.1ml, 0.15ml, and 0.2ml of ablation drugs were used. paclitaxel has a higher necrosis rate than the remaining groups (P<0.001) (Fig. 6 e). When the dose of ablation drug was 0.3ml, the difference of tumor necrosis rate among the five groups was statistically significant. The necrosis rate of paclitaxel and absolute ethanol group was higher than that of the other two groups (P<0.001) (Fig. 6 e). Our results indicated that the tumor ablation effect of the ethanol and paclitaxel groups was higher than that of the other ablative drugs. In addition, there was no statistical difference (P>0.05) in the percentages of necrosis caused by the ablative agents at doses of 0.2 mL and 0.3 mL in each group (Fig. 6 f). These data suggest that there is a threshold effect on the ablation effect. When the dosage of the ablation drug is greater than 0.2ml, the ablation effect cannot be improved by increasing the dose of the ablation agent.

Drug dispersion rate: The methylene blue tracing was observed and recorded in Fig. 6 g. The specific values and comparisons of blue-stained areas of each group are shown in Table 1, and Fig. 6 h, which showed statistical significance between the groups using analysis of variance (P<0.05). The results showed that paclitaxel diffused fastest in tumors, followed by ethanol and polidocanol, while lauromacrogol was the slowest.

Table 1: Specific values of blue-stained areas (mm^2) for each group for measuring the rate of drug dispersion.

Drugs Dosage	Anhydrous ethanol		lauromacrogol		Polidocanol		Paclitaxel	
	Left	Right	Left	Right	Left	Right	Left	Right
0.1mL	18.56	19.06	20.93	12.35	39.85	42.38	34.42	31.04
0.2mL	55.43	42.49	16.17	31.84	39.21	24.29	60.52	55.29
0.3mL	57.75	50.89	22.78	36.50	35.34	40.91	53.56	88.38

"Left" refers to the left side of the tumor divided in half in Fig. 6 g, while "right" refers to the right side of the tumors in the same Figure. The values are presented as area (mm^2) for all groups including Anhydrous ethanol, lauromacrogol, polidocanol, and paclitaxel groups to determine the rate of drug dispersion.

DISCUSSION

This study demonstrates the feasibility of ethanol-free ablation as an effective treatment for insulinomas. Through a prospective investigation using an animal model of insulinoma, we have assessed the viability, practicality, and safety of these drugs as ablative agents. Furthermore, we have evaluated the penetration and diffusion of different drugs within tumors, thereby establishing a theoretical foundation for the selection of effective, safe, and stable ablative agents for clinical applications.

Modern gene engineering techniques have facilitated the development of various pancreatic islet β-cell lines. Among these, the rat insulinoma (RIN) cell

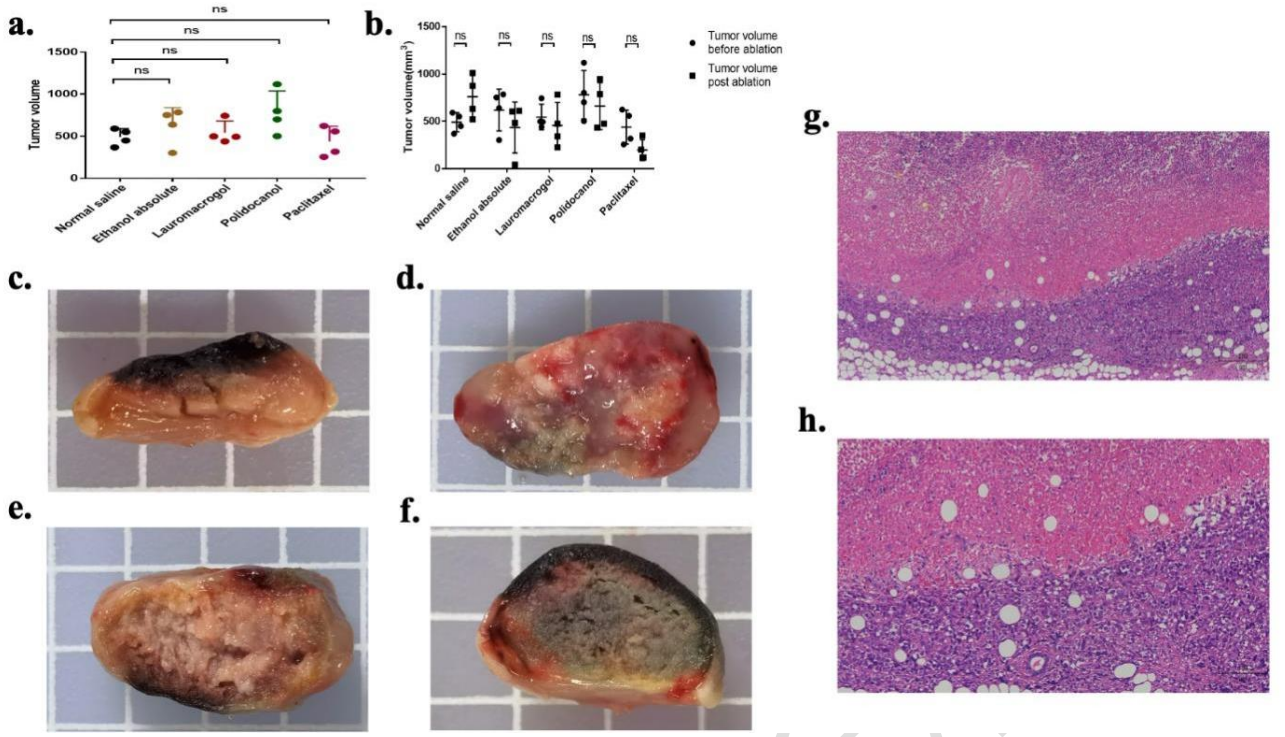

Fig. 5: Comparative analysis of tumors before and after ablation therapy. **a**. Scatter plot of tumor volumes before ablation in each group. **b**. Scatter plot showing changes in tumor volumes before and after ablation in each group. **c-f**. Macroscopic analysis of tumor necrosis 72 hours post-ablation at a 0.2 mL drug dose for each group. **c**. 0.2 mL ethanol: charred tumor surface with partial necrosis, adhering to smooth muscle tissue. **d**. 0.2 mL lauromacrogol: central necrotic tissue interwoven with residual tissue, a visible ablation zone, and local congestion. **e.** 0.2 mL polidocanol: central caseous necrosis with multiple fissures and no significant residual tumor necrosis. **f.** 0.2 mL paclitaxel: central caseous necrosis with multiple fissures, charred tumor surface, and no apparent residual necrosis. **g-h.** Light micrographs of hematoxylin & eosin staining in the EA group post-ablation (g= 100x; h= 200x)

line was one of the earliest established, originating from inbred NEDH rats subjected to high-dose radiation (Chick *et al*., 1977). The INS-1 subline of the RIN series, which maintains stable expression for over 80 passages, has been widely utilized for studying β-cell growth, survival factors, and the development of organoid or animal models (Schubert *et al*., 2013). In addition to RIN cell lines, the MIN cell line has also been reported as suitable for creating insulinoma mouse models. (Zheng *et al*., 2023; Chen *et al*., 2024). To date, most insulinoma animal models are based on experimental rodents. Immunodeficient BALB/c nude mice are commonly used as hosts for xenograft models, with tumor formation reported at various sites, including the adrenal gland, subrenal capsule, subcutaneous tissue, pancreas, and liver. Recently, genetically engineered mice have also been successfully utilized to establish insulinoma models. A classic modeling method involves transplanting rat RIN cell line cells (INS-1 or RIN-m5f) into the subrenal capsule of nude mice. This procedure necessitates a surgical incision on the kidney plane, isolation of the kidney outside the abdominal cavity, transplantation of the cells, and suturing the kidney back into place. Schubert U's team (Schubert *et al*., 2013) demonstrated that transplanting rat INS-1 cells into the adrenal gland of diabetic mice effectively established an insulinoma model. Similarly, Professor Collantes M (Collantes *et al*., 2017) successfully transplanted RIN-m5f cells into the left dorsal subcutaneous region of male athymic BALB/c nude mice. Functional rat insulin production by the subcutaneous tumors was confirmed by measuring blood glucose and C-peptide levels. Numerous studies worldwide have utilized this subcutaneous tumor model for research on radiation, pharmacology, and genetic studies (Detour *et al*., 2017; Murakami *et al*., 2021). In addition to the above modeling methods, the insulinoma model established by genetically engineered mice has also been adopted by more and more researchers in recent years (Bollard *et al*., 2018).

The subcutaneous tumor model is relatively simple and easy to observe. Therefore, we cultured the INS-1 and Min-6 cell lines, both of which have been successfully used in the literature to establish insulinoma nude mice models, and transplanted them subcutaneously into nude mice. Tumors became visible to the naked eye within 1 to 2 weeks and exhibited exponential growth. Once the tumor diameter reached approximately 0.8 to 1.0 cm, we removed food from the cages and replaced the bedding with non-nutritive materials to induce hypoglycemia in the mice through starvation tests. As the physiological function of the pancreatic islets in the experimental mice remained intact and the nude mice consumed food frequently, random blood glucose levels remained stable after tumor formation, with no spontaneous hypoglycemia observed. However, the starvation tests successfully induced hypoglycemia in the model group, accompanied by high plasma insulin peaks, closely resembling the blood glucose and insulin curve characteristics of clinical insulinoma patients. Pathological and immunohistochemical examinations further confirmed the success of the model. Ethanol is a well-established local ablative agent. However, its application in the treatment

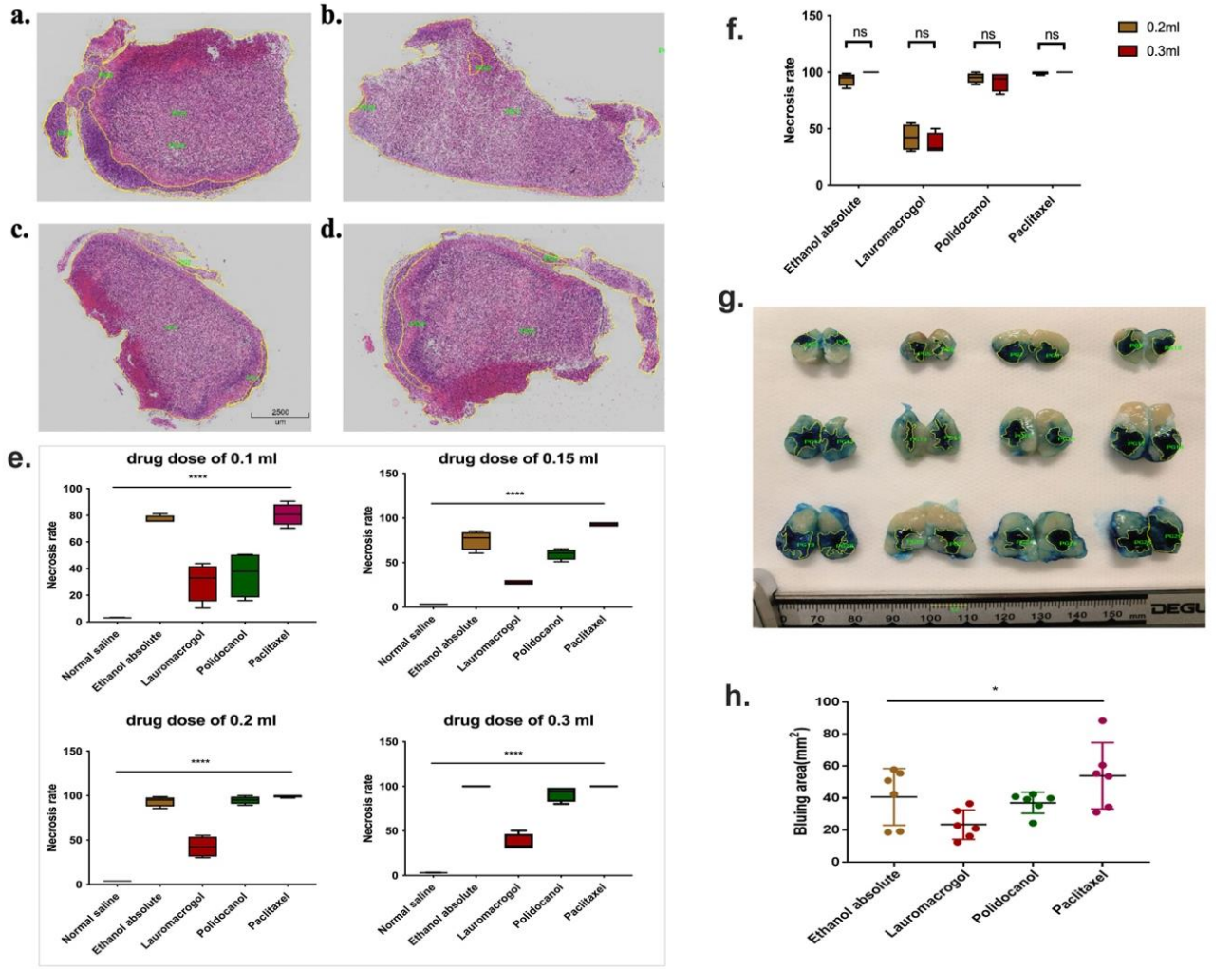

Fig. 6: Necrosis rates and drug diffusion analysis. **a-d.** Visualization of the whole tumor area and surviving tumor area in four samples from the same tumor (treated with 0.2mL ethanol ablation) under low magnification using Image-Pro Plus software. **e.** Box plot comparison of necrosis rates among groups using box plots treated with varying doses of ablation agents. **f.** Comparison of necrosis rates among groups treated with 0.2mL and 0.3mL ablation agents. **g.** Tumor sections dissected along the long axis with yellow sampling frames outlining dark, blue-stained areas for area calculation. **h.** Comparisons of the areas of blue staining areas (mm^2) among groups 30 minutes post-ablation.

of pancreatic lesions can result in uncontrollable adverse effects, such as pancreatitis and peritonitis. Extensive efforts have been made to enhance the effectiveness and safety of ablative therapy for insulinoma. Various drugs have been explored, including lauromacrogol, ethanol combined with poppy seed oil, and paclitaxel combined with gemcitabine (Choi *et al*., 2018; Qin *et al*., 2018; Gaballa *et al*., 2019). While successful cases have been reported for each of these drugs, the studies demonstrate considerable variability and a lack of comparative analysis (Schoemaker and van Zeeland, 2021). In recent years, the "ethanol-free" ablation technique has been shown to be safer and more effective for certain hepatic and pancreatic cystic lesions, demonstrating a reduced incidence of adverse reactions (Moyer *et al*., 2016; Moyer *et al*., 2017; An *et al*., 2022; Eso *et al*., 2022). Building on previous studies, we hypothesized that "alcohol-free" ablation could also be applicable to solid tumors of the pancreas. In this study, we established an insulinoma xenograft model in nude mice with endocrine functionality and conducted a series of ablative procedures on the tumors. The aim was to demonstrate that a diverse range of drugs, beyond traditional ethanol, can serve as local ablative agents for insulinomas and other solid pancreatic tumors. Based on the findings of this study, we concluded that paclitaxel and ethanol, administered at the same dosage, exhibited the highest efficacy in single ablation of subcutaneous insulinomas in nude mice, with no significant difference observed (93.20 ± 8.71% vs. 86.51 ± 11.92%). Additionally, polidocanol demonstrated the second-highest efficacy in tumor ablation.

Paclitaxel, a novel anti-microtubule agent, promotes the polymerization of microtubule protein dimers while inhibiting depolymerization. Consequently, it disrupts the normal dynamic reorganization of the microtubule network, which is essential for both interphase and mitotic cell functions. Studies have indicated that oral paclitaxel may serve as a chemotherapy option for malignant tumors in dogs, as it can reduce tumor size and improve clinical symptoms through mechanisms such as anti-angiogenesis, apoptosis, and cell cycle arrest (Chae *et al*., 2020; Yang *et al*., 2020). Additionally, one study demonstrated that paclitaxel could induce cellular toxicity, suggesting its potential use for the local ablation of liver tumors in rabbits. (Chen *et al*., 2021). However, in the paclitaxel group, nude mice exhibited reduced appetite and significant weight loss following drug administration, prompting us to consider potential systemic reactions

resulting from the local use of chemotherapeutic agents. Multiple studies have demonstrated that in the local chemical ablation of pancreatic cystic neoplasms (PCNs) using paclitaxel, no detectable blood drug concentrations were observed after injection into the PCNs. Systemic toxicities commonly associated with chemotherapy, such as myelosuppression, neurotoxicity, alopecia, and cachexia, were rarely observed with local application. (Oh *et al*., 2008; Oh *et al*., 2011; Attila *et al*., 2019; Canakis *et al*., 2020). This is because ablation therapy involves local injection under endoscopic ultrasound guidance, allowing for the concentration of the drug around the tumor without inducing systemic effects associated with intravenous administration. Furthermore, the systemic dose of paclitaxel used in chemotherapy for tumor patients can reach up to 175 mg/m², which far exceeds the doses reported for local ablation. Therefore, we conclude that when paclitaxel is used as an ablation agent in humans, its systemic effects remain within an acceptable range.

There is a paucity of large-scale clinical studies regarding the efficacy and safety of lauromacrogol as an ablative agent in tumor ablation therapy. However, current research suggests that lauromacrogol may exert a destructive impact on tumor tissues by generating thermal or cryogenic effects. Additionally, lauromacrogol has the potential to exhibit anti-tumor effects through mechanisms such as apoptosis induction and angiogenesis inhibition. It has demonstrated a clear therapeutic effect as an ablative agent for pancreatic cystic neoplasms (PCNs) and as a sclerosing agent for spider veins and varicose veins (Ardeshna *et al*., 2022; Gao *et al*., 2023; Min *et al*., 2023). Professor Qin from our research team (Qin et al., 2014) has reported relevant research on endoscopic ultrasound-guided ethanol ablation (EUS-EA) for the treatment of symptomatic insulinoma patients. For spherical tumors, the ethanol injection volume was set at half of the tumor's diameter. For elliptical or irregularly shaped tumors, the ethanol injection volume was calculated using the following formula: (long axis + short axis) / 2. If the tumor was located near blood vessels or the pancreatic duct, the ethanol injection volume was reduced to one-half or one-third of the standard volume. To mitigate some inevitable complications, such as abdominal pain and pancreatitis following EUS-EA, Professor Qin explored the use of lauromacrogol as an ablative agent in conjunction with this method. A total of 11 lesions in 7 patients with insulinoma were treated with endoscopic ultrasound-guided fine-needle injection (EUS-FNI), with a total of 16 procedures performed. After one or multiple sessions of polidocanol ablation, all patients experienced symptom relief, with normalization of blood glucose levels, improved insulin levels, and elevated C-peptide levels, and no adverse events were reported (Qin *et al*., 2018). Although this method demonstrated initial efficacy, many patients required repeated ablation to achieve effective symptom control. This observation led us to hypothesize that the single-session efficacy of polidocanol ablation is limited, particularly when the dosage is insufficient. The molecular formula of polidocanol is $C_{12}H_{25}(OCH_2CH_2)_nOH$, with a molecular weight of approximately 600 when n=9. While polidocanol has a similar molecular structure to that of lauromacrogol, the value of n in the molecular formula for polidocanol is more stable. When n ranges from 7.9 to 9.8, its molecular weight is approximately equal to that of lauromacrogol, which is around 400. In contrast, the value of n in the molecular formula for lauromacrogol is unstable, resulting in a variable molecular weight. Consequently, polidocanol exhibits higher stability and purity. To date, there have been no reports on the utilization of polidocanol for solid tumor ablation in humans or animals. However, its application in the treatment of cystic tumors has been documented. For instance, after two ultrasound-guided sclerotherapy treatments with polidocanol, the volume of thyroid cystic masses in geldings gradually decreased over six months, indicating that intralesional injection of polidocanol can serve as an effective sclerosing agent for cystic masses (Mageed *et al*., 2023). Additionally, reports have indicated that 1% polidocanol can be used as a sclerosing agent to treat mucous cysts in the orbits of dogs (Stuckey *et al*., 2012). Despite its molecular structure and pharmacological actions being similar to those of lauromacrogol, polidocanol exhibits greater stability and purity. Therefore, it is hypothesized that polidocanol may yield a superior ablative effect compared to lauromacrogol. This study aimed to verify this hypothesis and confirmed that polidocanol indeed demonstrated improved ablative efficacy. The group treated with polidocanol exhibited a higher percentage of necrosis following single ablation compared to the lauromacrogol group (70.48 ± 26.12% vs. 34.26 ± 0.72%). Additionally, adverse effects such as appetite loss and sudden weight reduction were observed in the paclitaxel group after drug administration, raising concerns about potential systemic reactions resulting from the topical application of chemotherapeutic agents. Considering that polidocanol has fewer systemic toxic and side effects than chemotherapy drugs, the prospect of its use in the clinic is still promising. More studies are needed to explore the ablation effectiveness and mechanism of polidocanol.

This study has several limitations. Firstly, the use of a nude mouse model imposes constraints on the drug's tolerability. Additionally, while this experiment provided preliminary insights into drug dosing, the experimental nude mice were limited by the amount of drug that could be administered, preventing an in-depth investigation of higher concentrations and larger doses. To address the differences in dosing between animal models and clinical applications, several approaches can be considered. These include refining dose calculation methods based on body weight, surface area, and anatomical differences between animal models and humans; utilizing physiologically-based pharmacokinetic modeling for more accurate predictions; conducting experiments on animal models that closely resemble human physiology, such as primates or larger animals, to enhance the translational relevance of findings; and employing advanced computer simulations and *in vitro* tissue models to predict optimal dosages and assess potential side effects. These methods can effectively complement animal studies and bridge the gap to clinical trials. Importantly, the amount of ablative drug used is primarily determined by the size of the tumor and the physical characteristics of the drug. Thus, the exact volume administered must be carefully calibrated to avoid systemic absorption while ensuring localized treatment.

Conclusions: In conclusion, INS-1 and MIN6 cells can successfully establish a subcutaneous insulinoma xenograft model in nude mice with intact endocrine function. This study established the feasibility and effectiveness of ethanol-free ablation for insulinomas, thus offering new therapeutic ideas and providing a theoretical foundation for clinical treatments.

Conflicts of interest: The authors have no conflicts of interest to declare.

Fundings: This work was supported by the Natural Science Foundation of Guangxi Zhuang Autonomous Region in China (Grant No. 81960439), the Innovative Research Group Project of the National Natural Science Foundation of China (Approval No. YYZS2020007), and Guangxi Medical and Health Appropriate Technology Development and Promotion Project (Approval No. S2024016).

Authors contributions: Nan Yi: Designed the subject, performed endoscopic procedures and wrote the manuscript. Fengping Chen: Performed endoscopic procedures and wrote the manuscript. Biaolin Zheng: Prepared the animal models. Wenwen Guo: Analysed data. Lin Yu: Designed and executed the animal experiments, including the care and handling of the animals. Haixing Jiang and Shanyu Qin: Acquired funds and revised the manuscript.

Availability of data and materials: All the data and materials will be available when requested. (Haixing Jiang, email address: Jianghaixing@gxmu.edu.cn)

Statement: We confirm the study is reported following ARRIVE guidelines.

REFERENCES

Tsang Y P, Lang B H and Shek T W, 2016. Assessing the short- and long-term outcomes after resection of benign insulinoma. ANZ J Surg 86:706-10.

Hawks D, Peterson M E, Hawkins K L, *et al*., 1992. Insulin-secreting pancreatic (islet cell) carcinoma in a cat. J Vet Intern Med 6:193-6.

Buishand F O, 2022. Current Trends in Diagnosis, Treatment and Prognosis of Canine Insulinoma. Vet Sci 9:540.

de Herder W W, Niederle B, Scoazec J Y, *et al*., 2006. Well-differentiated pancreatic tumor/carcinoma: insulinoma. Neuroendocrinol 84:83-8.

Greene S N and Bright R M, 2008. Insulinoma in a cat. J Small Anim Pract 49:38-40.

Bełtowski J, Wójcicka G and Jamroz-Wiśniewska A, 2018. Hydrogen sulfide in the regulation of insulin secretion and insulin sensitivity: Implications for the pathogenesis and treatment of diabetes mellitus. Biochem Pharmacol 149:60-76.

Ryan D, Pérez-Accino J, Gonçalves R, *et al*., 2021. Clinical findings, neurological manifestations and survival of dogs with insulinoma: 116 cases (2009-2020). J Small Anim Pract 62:531-539.

Kornya M, Abrams-Ogg A, Comeau D, *et al*., 2022. Juvenile hyperinsulinism in a Maine Coon kitten. JFMS Open Rep, 8: 205511692211364 73.

Varela D, Yu A and Saxon D, 2018. Insulinoma Masquerading as Transient Neurocognitive Impairment. Am J Med 131:e377-e379.

Scott A T and Howe J R, 2019. Evaluation and Management of Neuroendocrine Tumors of the Pancreas. Surg Clin North Am 99:793-814.

Sato S, Hori K, Tanabe G, *et al*., 2024. Effect of diazoxide on a cat with insulinoma. JFMS Open Rep 10:20551169231220290.

Hess L R, Ravich M L and Reavill D R, 2013. Diagnosis and treatment of an insulinoma in a guinea pig (Cavia porcellus). J Am Vet Med Assoc 242:522-6.

Yau W and Rissi D R, 2014. Cholecystic adenocarcinoma and pancreatic insulinomas in a goat. J Vet Diagn Invest 26:827-31.

Binici C, Plog S, Kershaw O, *et al*., 2016. Insulinoma in a 5-Year-Old Dexter Cow. J Vet Intern Med 30:1402-6.

Foxx J, Mans C, Strunk A, *et al*., 2022. Long-term medical management of insulinoma in a rabbit (Oryctolagus cuniculus). J Exot Pet Med 42:47-49.

Gómez Ochoa P, Alférez M D, de Blas I, *et al*., 2021. Ultrasound-Guided Radiofrequency Ablation of Chemodectomas in Five Dogs. Anim 11:2790.

Hendricks-Wenger A, Arnold L, Gannon J, *et al*., 2022. Histotripsy Ablation in Preclinical Animal Models of Cancer and Spontaneous Tumors in Veterinary Patients: A Review. IEEE Trans Ultrason Ferroelectr Freq Control 69:5-26.

Miwa Y, Kurosawa A, Ogawa H, *et al*., 2009. Neoplasitic diseases in ferrets in Japan: a questionnaire study for 2000 to 2005. J Vet Med Sci 71:397-402.

Jilesen A P, van Eijck C H, in't Hof K H, *et al*., 2016. Postoperative Complications, In-Hospital Mortality and 5-Year Survival After Surgical Resection for Patients with a Pancreatic Neuroendocrine Tumor: A Systematic Review. World J Surg 40:729-48.

Crinò S F, Napoleon B, Facciorusso A, *et al*., 2023. Endoscopic Ultrasound-guided Radiofrequency Ablation Versus Surgical Resection for Treatment of Pancreatic Insulinoma. Clin Gastroenterol Hepatol 21:2834-2843.

Qin S Y, Lu X P and Jiang H X, 2014. EUS-guided ethanol ablation of insulinomas: case series and literature review. Medicine (Baltimore) 93:e85.

Matsumoto K and Kato H, 2023. Endoscopic ablation therapy for the pancreatic neoplasms. Dig Endosc 35:430-442.

Mehrabi A, Fischer L, Hafezi M, *et al*., 2014. A systematic review of localization, surgical treatment options, and outcome of insulinoma. Pancreas 43:675-86.

Moyer M T, Sharzehi S, Mathew A, *et al*., 2017. The Safety and Efficacy of an Alcohol-Free Pancreatic Cyst Ablation Protocol. Gastroenterol 153:1295-1303.

Gaballa D, Abendroth C S and Moyer M T, 2019. Alcohol-free EUS-guided chemoablation of multiple pancreatic insulinomas. Endosc Int Open 7:E186-e188

Gallo G, Pietroletti R, Novelli E, *et al*., 2022. A multicentre, open-label, single-arm phase II trial of the efficacy and safety of sclerotherapy using 3% polidocanol foam to treat second-degree haemorrhoids (SCLEROFOAM). Tech Coloproctol 26:627-636.

Chick W L, Warren S, Chute R N, *et al*., 1977. A transplantable insulinoma in the rat. Proc Natl Acad Sci U S A 74:628-32.

Schubert U, Schmid J, Lehmann S, *et al*., 2013. Transplantation of pancreatic islets to adrenal gland is promoted by agonists of growth-hormone-releasing hormone. Proc Natl Acad Sci U S A 110:2288-93.

Zheng B, Chen X, Chen F, *et al*., 2023. 5-Iodotubercidin Inhibits the Growth of Insulinoma Cells by Inducing Apoptosis. Neuroendocrinol 113:641-656.

Chen F, Lu J, Zheng B, *et al*., 2024. Artesunate Inhibits the Growth of Insulinoma Cells via SLC7A11/ GPX4-mediated Ferroptosis. Curr Pharm Des 30:230-239.

Collantes M, Barajas M, Quincoces G, *et al*., 2017. Lessons from 11C-dihydrotetrabenazine imaging in a xenograft mouse model of rat insulinoma: is PET imaging of pancreatic beta cell mass feasible? Q J Nucl Med Mol Imaging 61:447-455.

Detour J, Pierre A, Boisson F, *et al*., 2017. Effect of Carbidopa on 18F-FDOPA Uptake in Insulinoma: From Cell Culture to Small-Animal PET Imaging. J Nucl Med 58:36-41.

Murakami T, Fujimoto H, Hamamatsu K, *et al*., 2021. Distinctive detection of insulinoma using [(18)F]FB(ePEG12)12-exendin-4 PET/CT. Sci Rep, 11: 15014.

Bollard J, Patte C, Massoma P, *et al*., 2018. Combinatorial Treatment with mTOR Inhibitors and Streptozotocin Leads to Synergistic *In Vitro* and *In Vivo* Antitumor Effects in Insulinoma Cells. Mol Cancer Ther 17:60-72.

Qin S, Liu Y, Ning H, *et al*., 2018. EUS-guided lauromacrogol ablation of insulinomas: a novel treatment. Scand J Gastroenterol 53:616-620.

Choi J H, Park D H, Kim M H, *et al*., 2018. Outcomes after endoscopic ultrasound-guided ethanol-lipiodol ablation of small pancreatic neuroendocrine tumors. Dig Endosc 30:652-658.

Moyer M T, Dye C E, Sharzehi S, *et al*., 2016. Is alcohol required for effective pancreatic cyst ablation? The prospective randomized CHARM trial pilot study. Endosc Int Open 4:E603-7.

An S, Sung Y N, Kim S J, *et al*., 2022. Pancreatic Cysts after Endoscopic Ultrasonography-Guided Ethanol and/or Paclitaxel Ablation Therapy: Another Mimic of Pancreatic Pseudocysts. Pathobiol 89:49-55.

Eso Y, Shimizu H, Takai A, *et al*., 2022. Ultrasound-guided polidocanol foam sclerotherapy for symptomatic giant hepatic cyst: A single-center experience. Hepatol Res 52:557-565.

Chae H K, Yang J I, An J H, *et al*., 2020. Use of oral paclitaxel for the treatment of bladder tumors in dogs. J Vet Med Sci 82:527-530.

Yang J I, Jin B, Kim S Y, *et al*., 2020. Antitumour effects of Liporaxel (oral paclitaxel) for canine melanoma in a mouse xenograft model. Vet Comp Oncol, 18: 152-160.

Chen L, Liu Z X, Bi Q C, *et al*., 2021. Ultrasound-Guided Percutaneous Ethanol-Paclitaxel Combined Therapy for Rabbit VX2 Liver Tumors. J Hepatocell Carcinoma 8:263-270.

Oh H C, Seo D W, Lee T Y, *et al*., 2008. New treatment for cystic tumors of the pancreas: EUS-guided ethanol lavage with paclitaxel injection. Gastrointest Endosc 67:636-42.

Oh H C, Seo D W, Song T J, *et al*., 2011. Endoscopic ultrasonography-guided ethanol lavage with paclitaxel injection treats patients with pancreatic cysts. Gastroenterol 140:172-9.

Attila T, Adsay V and Faigel D O, 2019. The efficacy and safety of endoscopic ultrasound-guided ablation of pancreatic cysts with alcohol and paclitaxel: a systematic review. Eur J Gastroenterol Hepatol 31:1-9.

Canakis A, Law R and Baron T, 2020. An updated review on ablative treatment of pancreatic cystic lesions. Gastrointest Endosc 91:520-526.

Gao F, Li H, Feng X, *et al*., 2023. Cystic tumor ablation with different concentrations of lauromacrogol solution in an animal model. Minerva Gastroenterol (Torino).

Ardeshna D R, Woods E, Tsung A, *et al*., 2022. An update on EUS-guided ablative techniques for pancreatic cystic lesions. Endosc Ultrasound 11:432-441.

Min X, Zhang Z, Chen Y, *et al*., 2023. Comparison of the effectiveness of lauromacrogol injection for ablation and microwave ablation in the treatment of predominantly cystic thyroid nodules: a multicentre study. BMC Cancer 23:785.

Mageed M, Steinberg T and Maleas G, 2023. Diagnostic imaging and conservative management of an ultimobranchial thyroid cyst in an adult horse. Equine Vet Educ 35:e14-e20.

Stuckey J A, Miller W W and Almond G T, 2012. Use of a sclerosing agent (1% polidocanol) to treat an orbital mucocele in a dog. Vet Ophthalmol 15:188-93.

Schoemaker NJ, and van Zeeland YR, 2021. Ferrets. Exotic Animal Emergency and Critical Care Medicine 201-237.

In-Press